PNAS
www.pnas.org

SI Appendix-Supplementary Information for

LXR directly regulates glycosphingolipid synthesis and affects human CD4+ T cell function

Kirsty E Waddington[a,b,1], George A Robinson[a], Beatriz Rubio-Cuesta[b,2], Eden Chrifi-Alaoui[a], Sara Andreone[a,3], Kok-Siong Poon[b,4], Iveta Ivanova[c], Lucia Martin-Gutierrez[a], Dylan M Owen[c,5], Elizabeth C Jury[a,#,*] and Inés Pineda-Torra[b,#,*].

[a] Centre for Rheumatology or [b] Centre for Cardiometabolic and Vascular Science, University College London, United Kingdom. [c] Department of Physics and Randall Division of Cell and Molecular Biophysics, King's College London, United Kingdom.

Present addresses: [1]GammaDelta Therapeutics Limited, London, UK, [2]Translational Oncology Laboratory, Research Institute i+12 and Spanish National Cancer Research Centre (CNIO) and Universidad Autonoma de Madrid, Madrid, Spain, [3]Department of Oncology and Molecular Medicine, Instituto Superiore di Sanità, 00161 Rome, Italy, [4]Department of Pathology, Yong Loo Lin School of Medicine, National University Singapore and [5]University of Birmingham, United Kingdom.

[#] Shared senior authorship
* Inés Pineda-Torra and Elizabeth C. Jury
Email: i.torra@ucl.ac.uk, e.jury@ucl.ac.uk

This PDF file includes:

Other supplementary materials for this manuscript include the following:

Supplementary Methods

Antibodies and reagents

Western blotting: Primary antibodies were anti-LXRα (clone PPZ0412, Abcam Cat# ab41902, RRID:AB_776094), anti-LXRβ (Active Motif Cat# 61178, RRID:AB_2614980), anti-phosphotyrosine (clone 4G10, Millipore Cat# 05-321, RRID:AB_309678) anti- phospho-LAT (Y191) (Cell Signaling Technology Cat# 3584, RRID:AB_2157728), anti-phospho CD3ζ (Y142) (clone EP265(2)Y, Abcam Cat# ab68235, RRID:AB_11156649), anti-p42/p44 MAPK(Thr202/204) (Cell Signaling Technology Cat# 9101, RRID:AB_331646) and anti-HSP90 (clone H-114, Santa Cruz Biotechnology Cat# sc-7947, RRID:AB_2121235). Horseradish peroxidase conjugated secondary antibodies were goat anti-rabbit IgG (Agilent Cat# P0448, RRID: AB_2617138 or Cell Signaling Technology Cat# 7074, RRID: AB_209923) or sheep anti-mouse IgG (GE Healthcare Cat# NA931, RRID: AB_772210).

Confocal microscopy: Primary antibodies were anti-phosphotyrosine (clone 4G10, Millipore Cat# 05-321, RRID: AB_309678) and anti-Lck (Santa Cruz Biotechnology Cat# sc-13, RRID: AB_631875). Secondary antibodies were goat anti-mouse IgG2b-AlexaFluor633 (Thermo Fisher Scientific Cat# A-21146, RRID: AB_2535782) and goat anti-rabbit IgG-AlexaFluor488 (Thermo Fisher Scientific Cat# A-11034, RRID: AB_2576217).

Flow cytometry: (i) Cholesterol and glycosphingolipid detection: CD4-BV711 (clone RPA-T4, BioLegend Cat# 300558, RRID:AB_2564393), CD25-BV510 (clone MA251, BD Biosciences Cat# 563351, RRID:AB_2744336), CD127-PEDazzle594 (clone A019D5, BioLegend Cat# 351336, RRID:AB_2563637), CD19-APC (clone HIB19, BioLegend Cat# 302212, RRID:AB_314242), CD14-efluor450 (clone 61D3, Thermo Fisher Scientific Cat# 48-0149-42, RRID:AB_1272050), cholera Toxin B subunit FITC conjugate (Sigma-Aldrich Cat# C1655), filipin complex from *Streptomyces filipinensis* (Sigma-Aldrich Cat# F9765, CAS: 11078-21-0). (ii) Lipid order experiments: CD4-BUV395 (clone SK3, BD Biosciences Cat# 563550, RRID: AB_2738273), CD25-APC (clone BC96, BioLegend Cat# 302610, RRID: AB_314280) and CD127-BV421 (clone A019D5, BioLegend Cat# 357424, RRID: AB_2721519), di-4-ANEPPDHQ (Thermo Fisher Scientific Cat# D36802). (iii) Intracellular staining: IFNγ-efluor450 (clone 4S.B3, Thermo Fisher Scientific Cat# 48-7319-42, RRID:AB_2043866), IL-4-APC (clone MP4-25D2, BioLegend Cat# 500812, RRID:AB_315131), IL-17A-AlexaFluor488 (clone eBio64Dec17, Thermo Fisher Scientific Cat# 53-7179-42, RRID:AB_10548943), IL-10-PE (clone JES3-19F1, BD Biosciences Cat# 554706, RRID:AB_395521), TNFα-BV421 (clone Mab11, BioLegend Cat# 502932, RRID:AB_10960738) and IL-2-FITC (clone 5344.111, BD Biosciences Cat# 340448, RRID:AB_400424). (iv) Proliferation: PE mouse anti-human Ki67 set (BD Biosciences Cat# 556027, RRID: AB_2266296) or Cell Trace Violet reagent (Invitrogen).

Fluorescence activated cell sorting (FACS): CD14-v450 (clone MφP9, BD Biosciences Cat# 560349, RRID: AB_1645559), CD8a-FITC (clone RPA-T8, BioLegend Cat# 301006, RRID: AB_314124), CD19-APC-Cy7 (clone SJ25C1, BD Biosciences Cat# 557791, RRID: AB_396873), CD4-BV605 (clone OKT4, BioLegend Cat# 317438, RRID: AB_11218995).

Cell culture

THP-1 cell line: The human monocytic THP-1 cell line was a gift from Jenny Dunne (UCL, UK). Cells were maintained at a density of 0.25 – 1x10^6/mL in complete media at 37°C, 5% CO_2. To induce monocyte to macrophage differentiation cells were plated at 0.4x10^6/mL) in complete media supplemented with 25 ng/mL phorbol 12-myrisate 13-acetate (PMA, Sigma) for 24 hours. Cells were washed and rested overnight prior to LXR activation.

Culture with LXR ligands: PBMCs or purified T cells were cultured in in 96 well plates (1 x10^6 cells/well) in complete media. Cells treated with GW3965 (GW) (1 μM, Sigma-Aldrich, CAS: 405911-17-3) were compared either to vehicle (dimethylsulfoxide, Sigma Cat# D2650), with the exception of RNA-sequencing experiments and di-4-ANEPPDHQ confocal imaging (Fig. 3d, S2n, S4h) where the LXR antagonist GSK1440233 (1 μM, GSK233) was used as control. 24S-hydroxycholesterol (10 μM, Enzo Cat# BML-GR230-0001, CAS: 474-73-7) and 24S,25-

epoxycholesterol (10 μM, Enzo Cat# BML-GR231-0001, CAS: 77058-74-3) were compared to vehicle (ethanol, Sigma Cat# E7023). The UGCG inhibitor N-Butyldeoxynojirimycin (NB-DNJ, Sigma Cat#B8299, CAS: 72599-27-0) was used at a final concentration of 10 μM, as in (1). For chromatin immunoprecipitation experiments, cells were also treated with RXR agonist LG100268 (LG) (100 nM, Sigma Cat# SML0279, CAS: 153559-76-3). For western blotting experiments cells were treated with LXR ligands for 48 hours, then serum starved (1% FBS) for 1 hour prior to TCR-stimulation in PBS for 2 – 10 minutes.

Functional assays: To activate the TCR, cells were stimulated with 1 μg/mL plate bound anti-CD3 (UCHT1, Thermo Fisher Scientific Cat# 16-0038-85, RRID: AB_468857) and 1 μg/mL anti-CD28 (CD28.2, Thermo Fisher Scientific Cat# 16-0289-81, RRID: AB_468926,) either in solution (for 72 hour cultures) or also plate bound (for stimulations <1 hour). For microscopy experiments glass-bottomed 8-well chamber slides (Ibidi) or dishes (WillCo-dish) were coated with 5 μg/mL anti-CD3 and anti-CD28 antibodies. To measure intracellular cytokine production cells were additionally stimulated with 50 ng/mL PMA (Sigma Cat# P1585) and 250 ng/mL ionomycin (Sigma Cat# I0634) for 5 hours with GolgiPlug (BDBiosciences Cat# 555029). Ionomycin dose was increased to 1 μg/mL for IL-17A production. Donors with negligible induction of cytokines or proliferation compared to unstimulated controls were excluded from analysis (n=2).

Chromatin immunoprecipitation

15 – 20 x10^6 PBMCs were rested overnight in complete media at 5x10^6/mL in 6-well plates. Cells were treated with 1 μM GW ± 100 nM LG for 2 hours, and then washed in cold PBS. Samples were double crosslinked, first with 2 mM disuccinimidyl glutarate (ThermoFisher Scientific, 20593, CAS: 79642-50-5) for 30 minutes at RT, followed by 10 minutes with 1% formaldehyde (Pierce 16% methanol free, ThermoFisher Scientific). Nuclei were isolated as previously described(2), and chromatin was sonicated for 12 cycles of 30s on and 30s off in an ultrasonic bath sonication system (Bioruptor Pico (Diagenode)). 6 μg of pre-cleared chromatin was immunoprecipitated with 2 μg/IP anti-Histone H3K27Ac (Abcam Cat#ab4729; RRID: AB_2118291), 4 μg/IP of anti-LXRα/β (provided by Knut Steffenssen, Karolinska Institute, Sweden) or 4 μg/IP anti-rabbit IgG control (Sigma-Aldrich Cat#I5006; RRID: AB_1163659). Two IPs were performed for LXR and pooled prior to DNA purification.

To identify potential LXRE sequences we used NHR scan (RRID:SCR_016975)(82) to interrogate the UGCG gene ±20kb, as in (2, 3). Cistrome DB was used to identify LXR ChIP-seq experiments (4, 5). Primer sequences are provided in Table S4.

Lipid extraction for mass spectrometry lipidomics. Lipids were extracted using a two-step chloroform/methanol procedure(6). Samples were spiked with internal lipid standard mixture containing: cardiolipin 16:1/15:0/15:0/15:0 (CL), ceramide 18:1;2/17:0 (Cer), diacylglycerol 17:0/17:0 (DAG), hexosylceramide 18:1;2/12:0 (HexCer), lyso-phosphatidate 17:0 (LPA), lyso-phosphatidylcholine 12:0 (LPC), lyso-phosphatidylethanolamine 17:1 (LPE), lyso-phosphatidylglycerol 17:1 (LPG), lyso-phosphatidylinositol 17:1 (LPI), lyso-phosphatidylserine 17:1 (LPS), phosphatidate 17:0/17:0 (PA), phosphatidylcholine 17:0/17:0 (PC), phosphatidylethanolamine 17:0/17:0 (PE), phosphatidylglycerol 17:0/17:0 (PG), phosphatidylinositol 16:0/16:0 (PI), phosphatidylserine 17:0/17:0 (PS), cholesterol ester 20:0 (CE), sphingomyelin 18:1;2/12:0;0 (SM), triacylglycerol 17:0/17:0/17:0 (TAG). After extraction, the organic phase was transferred to an infusion plate and dried in a speed vacuum concentrator. 1st step dry extract was re-suspended in 7.5 mM ammonium acetate in chloroform/methanol/propanol (1:2:4, V:V:V) and 2nd step dry extract in 33% ethanol solution of methylamine in chloroform/methanol (0.003:5:1; V:V:V). All liquid handling steps were performed using Hamilton Robotics STARlet robotic platform with the Anti Droplet Control feature for organic solvents pipetting.

Mass spectroscopy data acquisition. Samples were analyzed by direct infusion on a QExactive mass spectrometer (Thermo Scientific) equipped with a TriVersa NanoMate ion source (Advion

Biosciences). Samples were analyzed in both positive and negative ion modes with a resolution of Rm/z=200=280000 for MS and Rm/z=200=17500 for MSMS experiments, in a single acquisition. MSMS was triggered by an inclusion list encompassing corresponding MS mass ranges scanned in 1 Da increments(7). Both MS and MSMS data were combined to monitor CE, DAG and TAG ions as ammonium adducts; PC, PC O-, as acetate adducts; and CL, PA, PE, PE O-, PG, PI and PS as deprotonated anions. MS only was used to monitor LPA, LPE, LPE O-, LPI and LPS as deprotonated anions; Cer, HexCer, SM, LPC and LPC O- as acetate adducts.

Lipidomics data analysis. Data were analyzed with in-house developed lipid identification software based on LipidXplorer (8, 9). Data post-processing and normalization were performed using an in-house developed data management system. Only lipid identifications with a signal-to-noise ratio >5, and a signal intensity 5-fold higher than in corresponding blank samples were considered for further data analysis. Prior to statistical analysis lipid levels were normalised to total cell numbers, and lipids quantified in less than 3 out of 4 donors were removed, leaving 366 lipid species. The amounts in pmoles of individual lipid molecules (species of subspecies) of a given lipid class were summed to yield the total amount of the lipid class. The amounts of the lipid classes may be normalized to the total lipid amount yielding mol% per total lipids. Both pmol and mol% data were compared using paired t-tests. Fold changes represent the ratio of the mean of each treatment group.

RNA sequencing. Samples were processed using the NEB RNA Ultra II Directional assay with PolyA mRNA workflow (p/n E7760) according to manufacturer's instructions. Briefly, mRNA was isolated from 100ng total RNA using Oligo dT beads to pull down poly-adenylated transcripts. The purified mRNA was fragmented using chemical hydrolysis (heat and divalent metal cation) and primed with random hexamers. Strand-specific first strand cDNA was generated and "A-tailed" at the 3' end. Full length xGen adaptors (IDT), containing unique 8bp dual sample specific indexes, a unique molecular identifier and a T overhang are ligated to the A-Tailed cDNA. Successfully ligated cDNA molecules were then enriched with limited cycle PCR (13 cycles). Libraries to be multiplexed in the same run are pooled in equimolar quantities, calculated from Qubit and Bioanalyser fragment analysis. Samples were sequenced on the NextSeq 500 instrument (Illumina, San Diego, US) using a 43bp paired end run.

RNA sequencing data analysis. Run data were demultiplexed and converted to fastq files using Illumina's bcl2fastq Conversion Software v2.19. Samples were grouped by treatment or disease status. To establish differences in gene expression between groups, sequence reads were aligned using STAR v2.5.0b to the human hg19 reference genome. Gene count abundance was quantified using Partek E/M Annotation Model with default settings in Partek's RNA Flow software as in (2). Differential expression analysis was performed using DESeq2 option in RNA Flow, which uses the Benjamin-Hochberg method for multiple testing correction. Pathway enrichment analysis was performed using Metascape [http://metascape.org](10). Clustered heatmaps were generated in ClustVis [http://biit.cs.ut.ee/clustvis/](11), using correlation distance and average linkage for hierarchical clustering. Venn diagrams were generated with BioVenn [http://www.biovenn.nl/index.php](12).

Flow cytometry. $1x10^6$ PBMCs were stained with Zombie (BioLegend) or LIVE/DEAD (ThermoFisher Scientific) fixable viability dyes for 30 minutes at 4°C, then labelled with antibodies to surface markers in cell staining buffer (PBS, 1% FBS and 0.01% sodium azide) or Brilliant Stain buffer (BD Biosciences) for 30 minutes at 4°C. Plasma membrane lipids were analysed by flow cytometry, as previously described (13). All samples were acquired on BD LSR II or BD LSRFortessa X-20 cytometers using BD FACSDiva software. Compensation was performed using anti-mouse IgGκ/negative control compensation particles set (BD Bioscience) or OneComp eBeads (ThermoFisher Scientific), with the exception of viability dyes and filipin which were performed with single stained and unstained cells. Data was analysed using FlowJo (Tree Star). Geometric mean fluorescent intensities (gMFI) and/or percentages were exported for statistical analysis.

Cytokine Bead Array (CBA). $CD4^+$ T cells were stimulated with anti-CD3 and anti-CD28 for 72 hours and supernatants were harvested and stored at -20°C. The Human Th1/Th2/Th17 Cytokine Bead Array kit (BD Bioscience, 560484) was used to measure expression of IFN-gamma, TNF, IL-6, IL-2, IL-4, IL-10 and IL-17 in 25 L of undiluted supernatant. Sample were acquired on a BD FACSVerse. IFN-gamma levels exceeded the dynamic range of the assay. Values below the level of detection were removed, and outliers were identified using the ROUT method (Q=5%).

Total Internal Reflection Fluorescence (TIRF) microscopy. $CD4^+$ T cells were stained with 5 μM ANE at $1.5x10^6$ cells/mL in Hank's buffered saline solution (HBSS) with 20 μM HEPES for 30 minutes at 37°C. A Nikon Ti-E wide field microscope was used with a 1.49 NA x60 Apo-TIRF oil immersion Nikon objective, under TIRF conditions and an Andor sCMOS camera for signal capture. To record live cells stained with ANE a customised two-channel set up was used to simultaneously record signal from ordered and disordered membranes. 30-minute movies were acquired at a rate of 1 frame per minute. A 488 nm laser set to 40% power was used for the excitation. Emitted light was directed to a Cairn OptiSplit III 2-channel image splitter, equipped with a 605 nm dichroic mirror,and 542/50 nM and 660/52 nM bandpass filters. This separated the fluorescent signal into ordered (542/50) and disordered (660/52) channels prior to detection. A suitable correction lens and neutral density filter were used to ensure similar intensity in both channels.

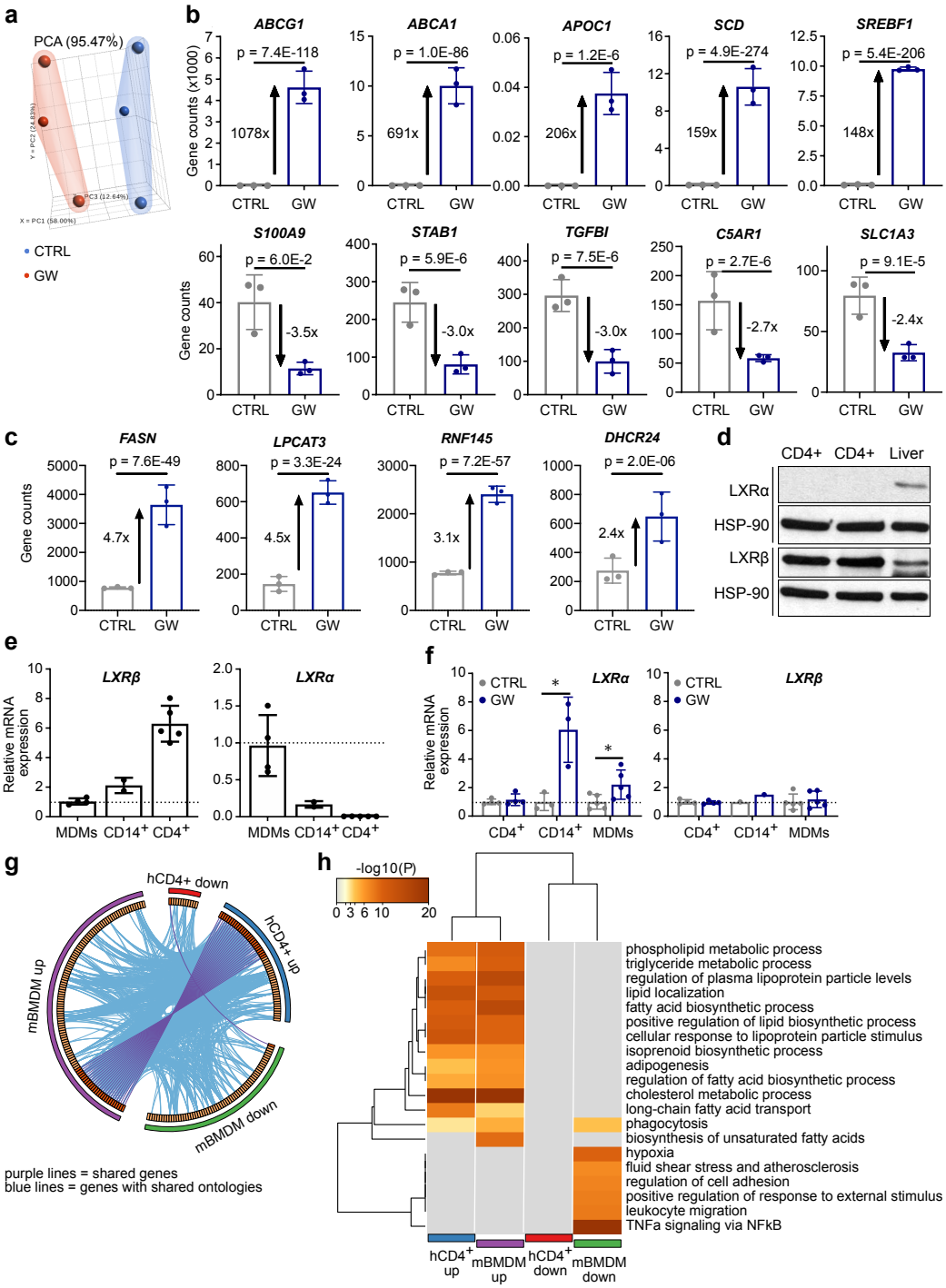

Fig. S1. (a) Principal component analysis (PCA) comparing RNA-seq data from CD4⁺ T cells treated with LXR agonist GW3965 (GW) for 24 hours to control (CTRL). **(b-c)** Normalised RNAseq gene counts for **(b)** the genes with the greatest response to GW stimulation and **(c)** known LXR target genes. **(d)** LXRα and LXRβ protein expression by Western blotting in CD4+ T cells (n=2) and human liver lysate with HSP90 loading control. **(e)** mRNA expression of LXRα and LXRβ was measured in cells from independent donors: human monocyte derived macrophages (MDMs) (n=4), CD14⁺ monocytes (n=2) or CD4⁺ T cells (n=5). Gene expression was normalized to cyclophilin A and expressed relative to MDMs (MDMs=1, shown by dashed line). **(f)** Human

immune cells were cultured with 1 μM GW for 16-18 hours (n=3-9). Expression of LXR subtypes was analysed by qPCR (CTRL=1, shown by dashed line). **(g-h)** Comparison of GW-regulated genes in human $CD4^+$ T cells and murine macrophages. The circos plot shows GW-regulated genes (purple lines) and functional pathways (blue lines) common to human $CD4^+$ T cells and murine bone marrow derived macrophages (BMDMs)(5). The clustered heatmap compares the statistical significance of the top 20 enriched pathways across the two cell types. **(b-d, f)** All histograms show mean ± SD. Unpaired two-tailed t-tests; *$p < 0.05$.

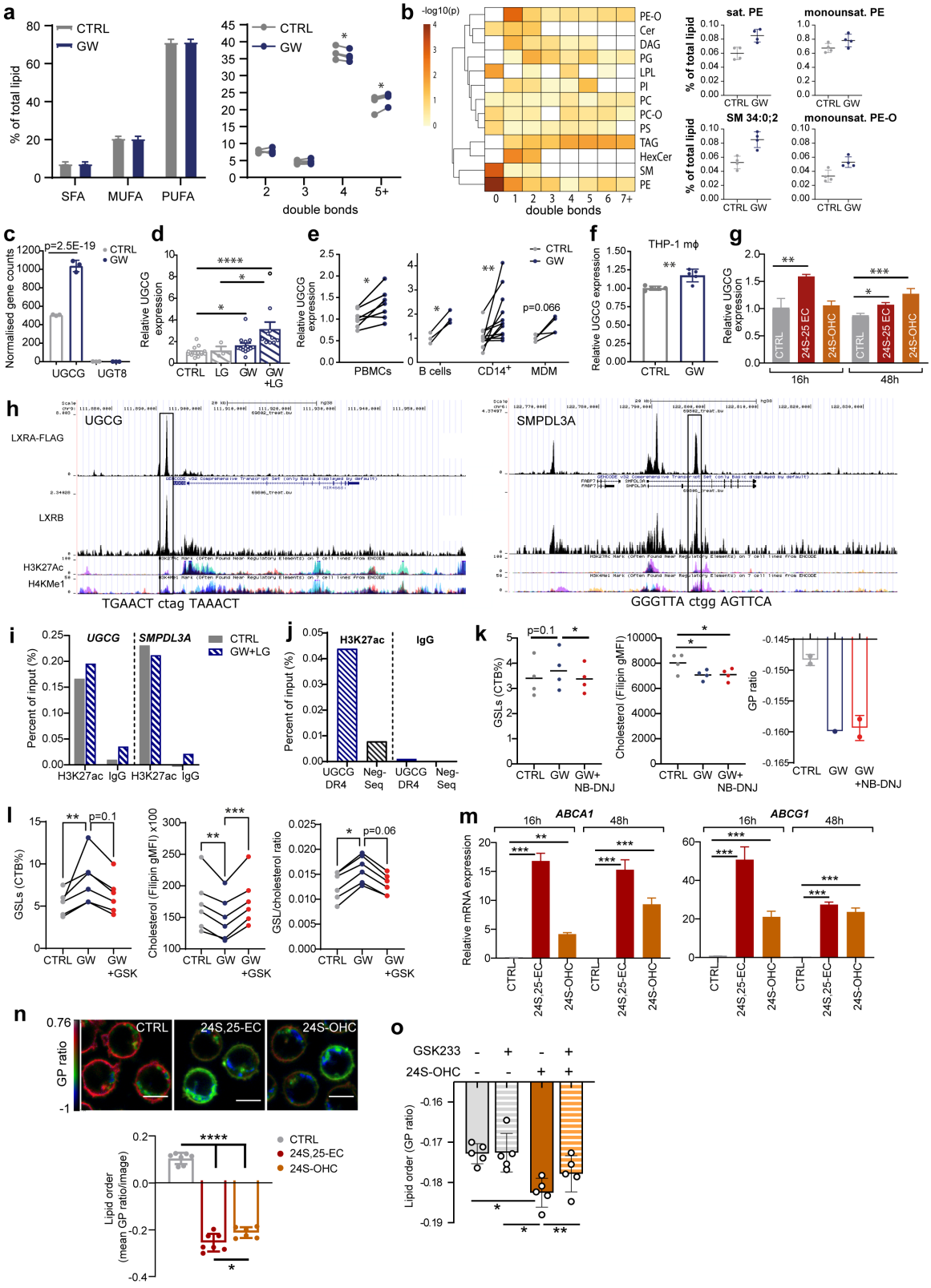

Fig. S2. (a-b) Lipid saturation was measured by shotgun lipidomics. Percentage of lipids with each degree of unsaturation was compared in total **(a)** and within each lipid class **(b)**. Heatmap shows p-values of comparisons made within subclasses with dot plots of the top hits. White

squares represent absent values. **(c)** Normalised RNA-Seq gene counts for UGCG and UGT8 and p-value from RNA-seq analysis. **(d-g)** UGCG mRNA expression was measured by qPCR. **(d)** $CD4^+$ T cells purified by MACS were treated with LXR (GW, 1 μM) and RXR (LG100268; LG, 100 nM) ligands. **(e)** PBMCs (n=7, 5 hours), B cells (n=3), CD14+ monocytes (n=12) and monocyte-derived macrophages (MDM) (n=4), **(f)** differentiated THP-1 macrophages were stimulated with GW and **(g)** T cells treated with endogenous LXR ligands 24S, 25-epoxycholesterol (24S-25 EC) or 24S-hydroxycholesterol (24S-OHC) compared to ethanol control (CTRL). **(h)** LXR occupancy in HT29 colorectal cancer cells treated with GW for 2 hours (10 μM)(14) and ENCODE data of histone marks commonly associated with regulatory sequences. Highlighted peaks labelled with putative DR4 sequences identified with NHR scan show regions amplified by ChIP-qPCR. **(i-j)** Cells were treated with LXR (GW, 1 μM) and RXR (LG100268; LG, 100 nM) ligands for 2 hours. **(i)** H3K27 acetylation at the putative DR4 motif at UGCG compared to IgG control and positive control (SMPDL3A) sequences. Representative of three independent experiments. **(j)** H3K27 acetylation at the *UGCG* DR4 motif compared to a negative control sequence and to IgG. Representative experiment shown. **(k)** Cholesterol, glycosphingolipid (GSL) levels (n=4) and lipid order (analysed with di-4-ANEPPDHQ, n=1) measured by flow cytometry in cells treated with GW ± UGCG inhibitor (NB-DNJ) for 24 hours. **(l)** Cholesterol, GSL levels and GSL:cholesterol ratio and lipid order in CD4+T cells treated with GW ± LXR antagonist (GSK233 - GSK) for 24 hours (n=6). **(m)** Induction of LXR target genes ABCA1 and ABCG1 was analysed by qPCR (n=3, pooled). **(n)** Membrane lipid order was analysed with di-4-ANEPPDHQ (n=1) by confocal microscopy and the mean GP ratio per image was quantified and compared. Scale bar represents 5 μM. **(o)** Cumulative data from three experiments showing lipid order measured by flow cytometry. Cells were treated with an LXR agonist (24S-OHC) ± LXR antagonist (GSK233)(n=5) for 24 hours. Data is shown as mean ± SD. **(a-b and e-f,i)** Two-tailed t-tests, **(d)** Kruskal-Wallis test or **(g,m)** One-way ANOVA with Dunnett's test and **(l,n,o)** One-way ANOVA with Tukey's posthoc test *$p < 0.05$, **$p < 0.01$, ***$p < 0.001$ and ****$p < 0.0001$.

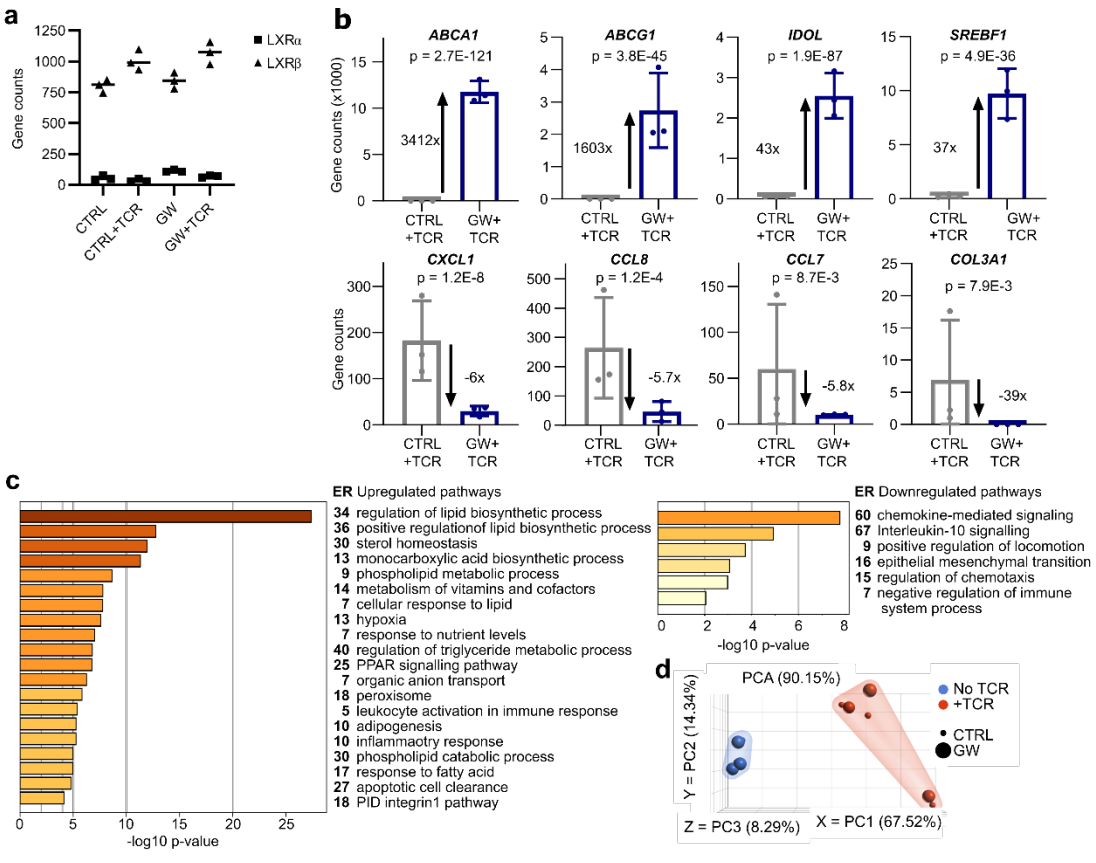

Fig. S3. RNA-seq was performed on CD4+ T cells (n=3) incubated ± GW for 6 hours, before stimulation with anti-CD3/CD28 (TCR) ± GW. **(a)** Normalised gene counts comparing the expression of LXRα and LXRβ and **(b)** of differentially expressed genes showing the strongest differences. **(c)** Pathway enrichment analysis of genes up- or down-regulated in GW+TCR compared to CTRL+TCR. Bar chart plots p-values and is annotated with the enrichment ratio (ER). **(d)** Principal component analysis (PCA) comparing TCR stimulated to unstimulated samples.

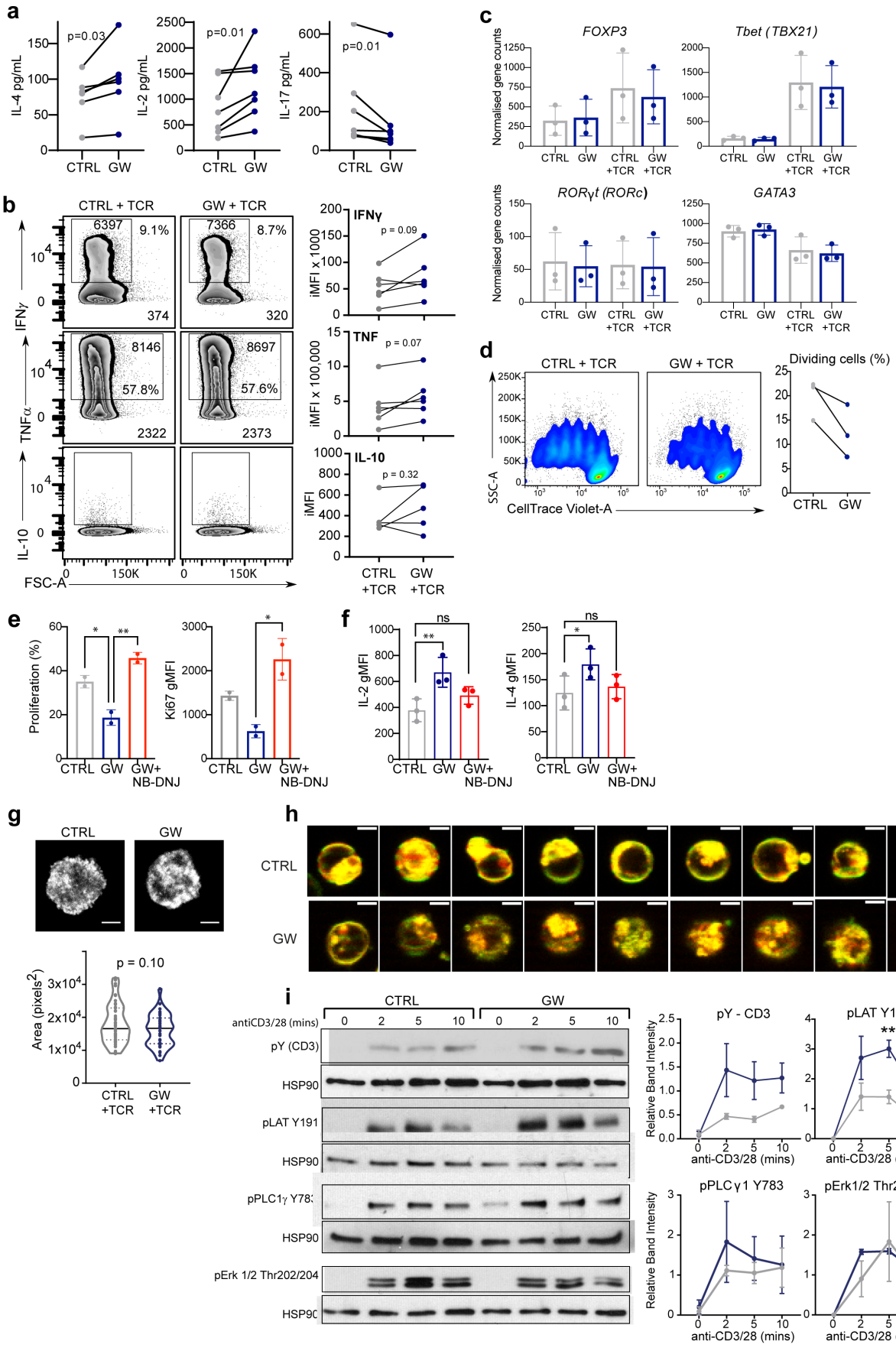
a
IL-4 pg/mL
p=0.03
IL-2 pg/mL
p=0.01
IL-17 pg/mL
p=0.01
CTRL GW
b
CTRL + TCR
GW + TCR
6397
9.1%
374
7366
8.7%
320
IFNγ
8146
57.8%
2322
8697
57.6%
2373
TNFα
IL-10
FSC-A
IFNγ
p = 0.09
TNF
p = 0.07
IL-10
p = 0.32
iMFI x 1000
iMFI x 100,000
iMFI
CTRL +TCR
GW +TCR
c
FOXP3
Tbet (TBX21)
RORγt (RORc)
GATA3
Normalised gene counts
CTRL GW CTRL +TCR GW +TCR
d
CTRL + TCR
GW + TCR
SSC-A
CellTrace Violet-A
Dividing cells (%)
e
Proliferation (%)
Ki67 gMFI
CTRL GW GW+ NB-DNJ
f
IL-2 gMFI
IL-4 gMFI
ns
g
CTRL
GW
p = 0.10
Area (pixels2)
h
CTRL
GW
i
CTRL
GW
antiCD3/28 (mins)
0 2 5 10
pY (CD3)
HSP90
pLAT Y191
pPLC1γ Y783
pErk 1/2 Thr202/204
pY - CD3
pLAT Y191
pPLCγ1 Y783
pErk1/2 Thr202/204
Relative Band Intensity
anti-CD3/28 (mins)

Fig. S4. (a-b) Magnetically-isolated $CD4^+$ T cells were activated with anti-CD3/CD28 (+TCR) for 72 hours in the presence of GW3965 (GW) or control (CTRL). **(a)** Cytokines secreted into cell-culture supernatants were measured by cytokine bead array (n=7-9). **(b)** Intracellular cytokine accumulation was analysed after additional treatment with PMA, ionomycin and GolgiPlug. Flow cytometry plots are labelled with percentages of cytokine-producing cells, and the geometric mean fluorescence intensities (gMFI) of both the cytokine-producing population (inside gate) and whole population (bottom left). Dot plots show cumulative data from 4 independent experiments. **(c)** Transcription factor gene expression measured by RNAseq (as in Fig.4). **(d-e)** Magnetically-isolated $CD4^+$ T cells were activated with anti-CD3/CD28 (+TCR) for 72 hours in the presence of GW3965 (GW) or control (CTRL). Proliferation was measured using dilution of CellTraceViolet (n=3) **(c)** or by Ki67 expression with the addition of the GSL biosynthesis inhibitor NB-DNJ **(d)**. **(f)** Dot plots show cumulative intracellular cytokine production in the presence of NB-DNJ**.** **(g)** $CD4^+$ T cells were activated with antibody coated coverslips for 10 minutes. Fixed synapses were stained with phalloidin and imaged by TIRF microscopy to assess the area of the cell-coverslip interface (n >16 cells/donor, n= 2 donors). Scale bar=5μM. **(h)** Magnetically purified $CD4^+$ T cells were cultured ± GW before addition to chamber slides coated with anti-CD3/28 for immune synapse formation. T cells were stained with di-4-ANEPPDHQ and confocal images taken at 15 minutes post activation using confocal microscopy. Nine representative images from control and GW-treated cells from one representative experiment of three. Scale bar=5μM. **(i)** Signaling protein phosphorylation after 2, 5 and 10 minutes of TCR engagement by Western blotting. Band intensities relative to HSP-90 (as loading control) were calculated for 2-3 independent experiments (n=2-4 donors). Two-tailed Wilcoxon tests **(a)**, t-tests **(b,d,g,i)** or One-way ANOVA with Tukey's post-hoc test **(c,e,f)**: *$p<0.05$, **$p<0.01$. Abbreviations: Lck – lymphocyte-specific protein tyrosine kinase; pY – phosphotyrosine; CD3 – cluster of differentiation 3; LAT – linker for activation of T cells; PLCγ – phospholipase Cγ1; Erk – extracellular signal related kinase; HSP90 – heat shock protein 90.

Table S1. Identification of novel LXR-regulated transcripts. To determine whether genes had previously been linked to LXR a literature search conducted in PubMed using terms 'LXR', 'NR1H2', 'NR1H3' and gene symbols. The T-cell only gene list was also cross-referenced with published data from human macrophages(15), THP-1 cells(16) and BMDMs(17).

No direct link to LXR identified	BRWD3, CHD2, MKNK2, SLC29A2, TDRD6, TGFBI, TKT, UGCG
Evidence of LXR regulation	IFI30, CD14 and C5AR1(17), S100A9(18), AQP9(19), MSMO1(20), ABCD1(16), MMAB(15), ACSL1(21)
Evidence of species-specific LXR regulation	SMPDL3A(16), OLMALINC(22), IL1RN(15), TGFBI(15)

Table S2. Interaction of LXR and TCR activation on gene expression. LXR-regulated genes were hierarchically clustered, and four distinct patterns of gene expression were identified based on their response to LXR activation with GW3965 and T cell receptor stimulation (anti-CD3/28). For each cluster (A-D) the responses to LXR ligand (LXR) and TCR stimulation (TCR) are summarized and all genes within the cluster are listed.

Cluster A LXR: up TCR: none	RDH11, SLC25A1, STX1A, LILRA1, LINC01578, C3, STARD4, CLCN6, MYLIP, SREBF1, ABCA1, INSIG1, ABCD1, ACSL3, TMEM135, ABCG1, MID1IP1, SCD, BRWD3, OLMALINC, RARA, FADS1, FADS2
Cluster B LXR: up TCR: down	APOE, SMPDL3A, LSS, MKNK2, NR1H3, SLC29A2, EEPD1, CD14, TLR4, FBP1, IDH1, FGR, KMO, SDC2, ALDOC, GAPT, CORO7, LOC100130872, BLOC1S1-RDH5, LEF1, ZNF775
Cluster C LXR: up TCR: up	ISY1-RAB43, TNFSF15, PLAUR, TGM2, ADM, UGCG ATP5J2-PTCD1, METTL9, SREBF2, LDLR, LPCAT3, MVD, RNF145, GPR82, PCYT2, PRDX5, ACACA, DBI DHCR7, FASN, MMAB, MVK, FDPS, TNC, IL1RN, TCF15, TMEM160, LIPG, ZBTB10, FAM213A, OLR1
Cluster D LXR: down/none TCR: up/down	SLFN12L, SUCNR1, ACOD1, LNPEP, MSH5, PHOSPHO2-KLHL23, CCL2, CCL7, CCL8, COL3A1, PCDH7, TENM4, DOCK4, CXCL1, CXCL2, LRRC24, RPS10-NUDT3, GNRHR, ZNF66, LOC100507053, SAMD12, CORO7-PAM16, LOC101593348, TGFBI, TNS3, MIAT, TRIM39-RPP21

Table S3. Oligonucleotide sequences for qPCR.

Gene	Forward primer (5'-3')	Reverse primer (5'-3')
ABCA1	TGAGCTACCCACCCTATGAACA	CCCCTGAACCCAAGGAAGTG
ABCG1	TGCAATCTTGTGCCATATTTGA	TGCAATCTTGTGCCATATTTGA
Cyclophilin A (*PPIA*)	GCATACGGGTCCTGGCATCTTGTCC	ATGGTGATCTTCTTGCTGGTCTTGC
FASN	CTGCTGCTGGAAGTCACCTA	GTGTGTGTTCCTCGGAGTGA
LXRα (*NR1H3*)	AGAGGAGGAACAGGCTCATG	AAAGGAGCGCCGGTTACACT
LXRβ (*NR1H2*)	GGAGCTGGCCATCATCTCA	GTCTCTAGCAGCATGATCTCGGATAGT
OLMALINC*	GACTCCTTTGG GAGACCAGTG	AGGTCACAGGGGATTTGATGG
SCD	GCAAACACCCAGCTGTCAAA	GCACATCATCAGCAAGCCAG
SREBP1c (*SREBF1*)	TCAGCGAGGCGGCTTTGGAG	CATGTCTTCGATGTCGGTCAG
UGCG	CGTCCTCTTCTTGGTGCTGT	AGAGAGACACCTGGGAGCTT

*Oligonucleotide sequences from (23).

Table S4. Oligonucleotide sequence for ChIP-qPCR.

Target	Forward primer (5'-3')	Reverse primer (5'-3')
UGCG DR4	ACTCTAGTCACTCCCCTGGAC	GCCTGATCTTGATAAACCACTGG
SMPDL3A LXRE*	TGCAATCTTGTGCCATATTTGA	TGCAATCTTGTGCCATATTTGA

*Oligonucleotide sequences from (16).

Lipid class	CTRL (pmol)	GW (pmol)	*P*-value	CTRL (%)	GW (%)	*P*-value
	Mean ± SD		paired	Mean ± SD		paired
Cholesterol esters	14 ± 5	9 ± 1	0.220	0.06 ± 0.02	0.04 ± 0.00	0.111
Ceramide	60 ± 22	54 ± 11	0.411	0.28 ± 0.07	0.25 ± 0.05	0.065
Cardiolipin	251 ± 96	286 ± 112	0.138	1.3 ± 0.6	1.4 ± 0.7	0.289
Diacylglycerol	131 ± 23	142 ± 29	0.491	0.6 ± 0.1	0.7 ± 0.1	0.475
Hexosylceramide	20 ± 4	27 ± 2	**0.017**	0.10 ± 0.01	0.12 ± 0.01	**0.005**
Lysophospholipid	14 ± 1	13 ± 3	0.370	0.07 ± 0.01	0.06 ± 0.02	**0.032**
Phosphatidate	10 ± 1	13 ± 4	0.231	0.05 ± 0.01	0.06 ± 0.02	0.324
Phosphatidylcholine	7023 ± 1329	6980 ± 1764	0.958	33 ± 3	32 ± 6	0.478
Phosphatidylcholine-ether	346 ± 57	336 ± 74	0.788	1.6 ± 0.2	1.5 ± 0.2	0.184
Phosphatidylethanolamine	2212 ± 509	2352 ± 636	0.538	10 ± 2	11 ± 2	0.377
Phosphatidylethanolamine-ether	2350 ± 355	2548 ± 418	0.215	11 ± 1	12 ± 1	0.141
Phosphatidylglycerol	60 ± 14	66 ± 15	0.501	0.28 ± 0.05	0.30 ± 0.05	0.374
Phosphotidylinositol	3509 ± 694	3664 ± 626	0.307	17 ± 3	17 ± 4	0.638
Phosphatidylserine	3767 ± 668	3820 ± 663	0.886	18 ± 3	18 ± 5	0.998
Sphingomyelin	1249 ± 184	1333 ± 106	0.220	5.9 ± 0.4	6.2 ± 0.4	0.553
Triacylglycerol	38 ± 13	113 ± 46	**0.032**	0.18 ± 0.05	0.51 ± 0.17	**0.013**

Table S5. FACS-sorted $CD3^+$ T cells were cultured ± GW3965 (GW) for 36 hours (n=4). Lipid concentrations are given in pmol and expressed as a percentage of the total lipid content (%). Samples were compared by a paired two-tailed t-test; $p < 0.05$ are bold. The average co-efficient of variance for each variable was used to determine the appropriate number of significant figures to display.

Movie Legends S1-2 (separate files). Control (Movie S1) or GW-treated (Movie S2) $CD4^+$ T cells stained with di-4-ANEPPDHQ and added to chamber slides coated with anti-CD3/28. Immune synapse formation was captured for 30 minutes at 60-second intervals using TIRF microscopy. Videos are pseudocoloured to show the generalized polarization (GP) ratio – a measure of lipid order (see scale below).

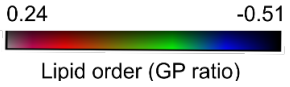

Dataset S1 (separate file). List of differentially expressed genes and Metascape pathway analysis results for GW vs GSK233 comparison.

Dataset S2 (separate file). List of differentially expressed genes and Metascape pathway analysis results for GW+TCR vs GSK233+TCR comparison.

References

1. G. McDonald *et al.*, Normalizing glycosphingolipids restores function in CD4+ T cells from lupus patients. *J Clin Invest* **124**, 712-724 (2014).
2. M. C. Gage *et al.*, Disrupting LXRα phosphorylation promotes FoxM1 expression and modulates atherosclerosis by inducing macrophage proliferation. *Proc Natl Acad Sci U S A* **115**, E6556-e6565 (2018).
3. N. Becares *et al.*, Impaired LXRα Phosphorylation Attenuates Progression of Fatty Liver Disease. *Cell Rep* **26**, 984-995.e986 (2019).
4. R. Zheng *et al.*, Cistrome Data Browser: expanded datasets and new tools for gene regulatory analysis. *Nucleic Acids Res* **47**, D729-d735 (2019).
5. S. Mei *et al.*, Cistrome Data Browser: a data portal for ChIP-Seq and chromatin accessibility data in human and mouse. *Nucleic Acids Res* **45**, D658-d662 (2017).
6. C. S. Ejsing *et al.*, Global analysis of the yeast lipidome by quantitative shotgun mass spectrometry. *Proceedings of the National Academy of Sciences* **106**, 2136-2141 (2009).
7. M. A. Surma *et al.*, An automated shotgun lipidomics platform for high throughput, comprehensive, and quantitative analysis of blood plasma intact lipids. *Eur J Lipid Sci Technol* **117**, 1540-1549 (2015).
8. R. Herzog *et al.*, LipidXplorer: a software for consensual cross-platform lipidomics. *PLoS One* **7**, e29851 (2012).
9. R. Herzog *et al.*, A novel informatics concept for high-throughput shotgun lipidomics based on the molecular fragmentation query language. *Genome Biol* **12**, R8 (2011).
10. Y. Zhou *et al.*, Metascape provides a biologist-oriented resource for the analysis of systems-level datasets. *Nature Communications* **10**, 1523 (2019).
11. T. Metsalu, J. Vilo, ClustVis: a web tool for visualizing clustering of multivariate data using Principal Component Analysis and heatmap. *Nucleic Acids Res* **43**, W566-570 (2015).
12. T. Hulsen, J. de Vlieg, W. Alkema, BioVenn - a web application for the comparison and visualization of biological lists using area-proportional Venn diagrams. *BMC Genomics* **9**, 488 (2008).
13. K. E. Waddington, I. Pineda-Torra, E. C. Jury, Analyzing T-Cell Plasma Membrane Lipids by Flow Cytometry. *Methods Mol Biol* **1951**, 209-216 (2019).
14. D. Savic *et al.*, Distinct gene regulatory programs define the inhibitory effects of liver X receptors and PPARG on cancer cell proliferation. *Genome Med* **8**, 74 (2016).

15. E. D. Muse *et al.*, Cell-specific discrimination of desmosterol and desmosterol mimetics confers selective regulation of LXR and SREBP in macrophages. *Proc Natl Acad Sci U S A* **115**, E4680-e4689 (2018).
16. P. B. Noto *et al.*, Regulation of sphingomyelin phosphodiesterase acid-like 3A gene (SMPDL3A) by liver X receptors. *Mol Pharmacol* **82**, 719-727 (2012).
17. A. Ramón-Vázquez *et al.*, Common and Differential Transcriptional Actions of Nuclear Receptors Liver X Receptors α and β in Macrophages. *Mol Cell Biol* **39** (2019).
18. L. Zhong, Q. Yang, W. Xie, J. Zhou, Liver X receptor regulates mouse GM-CSF-derived dendritic cell differentiation in vitro. *Mol Immunol* **60**, 32-43 (2014).
19. Y. B. Dai *et al.*, Liver X receptors regulate cerebrospinal fluid production. *Mol Psychiatry* **21**, 844-856 (2016).
20. C. L. Pinto *et al.*, Lxr regulates lipid metabolic and visual perception pathways during zebrafish development. *Mol Cell Endocrinol* **419**, 29-43 (2016).
21. S. J. Bensinger *et al.*, LXR signaling couples sterol metabolism to proliferation in the acquired immune response. *Cell* **134**, 97-111 (2008).
22. J. N. Benhammou *et al.*, Novel Lipid Long Intervening Noncoding RNA, Oligodendrocyte Maturation-Associated Long Intergenic Noncoding RNA, Regulates the Liver Steatosis Gene Stearoyl-Coenzyme A Desaturase As an Enhancer RNA. *Hepatol Commun* **3**, 1356-1372 (2019).
23. J. D. Mills *et al.*, High expression of long intervening non-coding RNA OLMALINC in the human cortical white matter is associated with regulation of oligodendrocyte maturation. *Mol Brain* **8**, 2 (2015).